Diffraction of *P* by the Core: A Study of Long-Period Amplitudes near the Edge of the Shadow

ROBERT A. PHINNEY AND LAWRENCE M. CATHLES

Department of Geological and Geophysical Sciences, Princeton University Princeton, New Jersey 08540

Theoretical expressions for the amplitude of *P* waves in the neighborhood of the core shadow boundary have been formulated and evaluated by computer. Comparison with 2.5-sec data of Sacks confirms his determination of the shadow position at 96.5°. A square-root frequency scaling law is found for the high-frequency diffraction pattern and permits the use of the Fresnel integral function at short periods. Long-period amplitude data for three paths have been spectrum-analyzed and compared against the theoretical amplitude dropoff going into the shadow. The agreement is about as good as the data will permit, and no indication is found at these periods of a low-amplitude defocused region at 90° to 96°, after diffraction has been accounted for.

INTRODUCTION

The penetration of long-period *P* waves deep into the optical shadow of the core by diffraction is a familiar demonstration that the amplitudes predicted by geometrical optics do not apply for a wide range of periods. The work reported here is part of a larger study aimed at developing useful wave-theoretical models of body-wave amplitudes near singularities of the travel-time curves. The specific problem of the core shadow is recognizably analogous to familiar problems of mathematical physics, namely the shadowing of light by an opaque screen and the diffraction of waves around a sphere.

Mathematical techniques appropriate to the problem of diffraction by a sphere were developed by *Watson* [1918] and by Van der Pol and Bremmer in a series of papers [*Bremmer*, 1949]. *Scholte* [1956] and *Duwalo and Jacobs* [1956] first applied these ideas to the elastic-wave problem, and *Nussenzweig* [1965] treated the basic acoustic diffraction problem with great thoroughness, giving asymptotic solutions for all the relevant receiver positions. *Teng and Wu* [1968] have worked with a two-dimensional ultrasonic model, providing analog solutions that agree with results given in this paper.

The simplest kinematical property of the core diffraction is the spatial decay constant of the wave which illuminates the deep shadow by propagation along the core-mantle interface. *Phinney and Alexander* [1966] obtained theoretical curves for this parameter for various models of the core-mantle boundary. *Alexander and Phinney* [1966] investigated the frequency dependence of the decay constant for long-period data from a selection of earthquakes. The principal results of these two papers were:

1. The determination that rigidity in the core has no significant effect on the decay constant, for the low rigidities known to be present.
2. The presence of apparent resonance maxima in the decay constant as a function of frequency for a group of paths over the Pacific, and the absence of this effect for a path from South America to Europe. Interpretation in terms of a transitional region at the core-mantle interface suggested a reduced shear velocity and increased density with respect to the mantle.

Serious questions still exist regarding this interpretation, connected with the repeatability of the results and the sensitivity of the results to stations with inadequately calibrated response (including a local geological correction). Whereas two more profiles will be discussed in this paper, a more comprehensive study will be

presented in a separate paper (Alexander and Phinney, in preparation).

In this paper we discuss the behavior of the P-wave amplitude at distances spanning the optical shadow position. We present calculations of the theoretical amplitude decay in this region and discuss the amplitude and phase velocity effects that arise from the diffraction. Some estimate can be made of the frequency and distance ranges for which ordinary ray theory and conventional time-domain amplitude analysis are valid. The distance of the optical shadow is estimated from published short-period data and confirms *Sacks'* [1966] determination of about 96.5°. A comparison of the theoretical amplitudes with an approximation based on diffraction by an opaque screen provides a usable amplitude function for high frequencies ($f > 0.12$ Hz).

For comparison, long-period data from two earthquakes, spanning three paths, have been frequency-analyzed and plotted as residuals against the theoretical amplitudes. The agreement is found to be quite good, although small effects are found which may be connected with departures from a simple model of the interface. Further study of these effects will require far better interstation calibration (including a crustal correction) and simultaneous determination of a source mechanism model. Since no provision is made in this paper for velocity variation in the mantle, we have not modeled the reversal in velocity gradient at the base of the mantle. This reversal is indicated by the observed amplitude drop beyond 85° assuming a geometrical optical mechanism. The lack of an amplitude residual in this range for long periods suggests that diffraction accounts fully for the long-period amplitude drop. Our results, therefore, do not seem to require any basal mantle structure to provide additional defocusing. The low resolution provided by the long periods does not make this an especially strong result, however.

Theory

Assume an earth consisting of a homogeneous elastic mantle and a homogeneous liquid core. With the origin of spherical coordinates at the center of the earth, the representation of a compressional point source at the surface is [*Morse and Feshbach*, 1953, p. 887]

$$\Phi_0 = \frac{e^{ikR}}{ikR} = \sum_{n=0}^{\infty} (2n + 1) P_n(\cos\theta) h_n^{(1)}(k_0 b) \hat{j}_n(k_0 r) \tag{1}$$

In discussing diffraction by the core, the outer boundary of the earth may be ignored, provided that the frequency is high enough for rays to be separated in the time domain. The diffracted signal, which includes both the incident wave and the generalized reflection from the core, is then

$$\Phi = \frac{1}{2} \sum_{n=0}^{\infty} (2n + 1) P_n(\cos\theta) h_n^{(1)}(k_0 b) \cdot [h_n^{(2)}(k_0 r) + C_0' h_n^{(1)}(k_0 r)] \tag{2}$$

By applying a modification of the transformation of *Watson* [1918], we may write the diffraction as a sum of forward- and backward-traveling waves that have made m circuits of the origin. For the forward-traveling wave with $m = 0$ we have

$$\Phi = \int_{-\infty}^{\infty} Q_{\nu-1/2}^{(2)}(\cos\theta) \frac{N(\nu)}{D(\nu)} \nu \, d\nu \tag{3}$$

By taking the asymptotic forms of the various expressions in the integrand for large ν and fixed ka, we find that all the terms except $m = 0$ can be evaluated by moving the contour into the upper half-plane and writing the integral as a sum of residues. The residue sum associated with the mth term is a 'creeping wave' that has made m transits of the origin, along the core-mantle boundary at the mantle P velocity. The $m = 0$ term can be written as a convergent residue sum only if the receiver is in the geometrical shadow of the core, in which case, the term represents the principal diffracted P wave in the shadow, having made less than one complete trip around the origin. If the receiver is in the illuminated zone, examination of the asymptotic form of (3) reveals two saddle points on the real ν axis, which correspond to the reflected and direct waves. When the receiver is very close to the shadow boundary, these saddle points approach each other. Formal discussion of this signal is possible only for frequencies high enough so that the asymptotic expansions can be relied upon.

Because of our desire to have reliable numeri-

cal results and to generalize them to a core-mantle boundary having layers or other radial structure, we have programmed (3) directly on the IBM 7094 and evaluated it by line integration along an optimum path. The path is generally arranged to be a steepest descent path at its extrema and to connect the two saddle points along the real axis. Since line integration is suitable for (3) even if the receiver is in the shadow, we routinely continue the evaluation into the shadow zone, where we can compare the result with the residue theory for the first pole. Typical maps of the complex plane are shown in Figure 1. The saddle points and steepest descent contours are indicated, and the function contoured is the Re[ln (integrand)], which is just the function whose steepest descent is of interest.

Because of the constant phase along the steepest descent paths, a Simpson or other low-order integration method is adequate. The variable phase between the two saddle points is not a severe limitation, provided that the two points are not too separated. When they are separated, the signals P and PcP are sufficiently distinct in time that this combined approach is unnecessary. For example, at a fixed distance from the shadow, the frequency can be made high enough so that the two saddle points are distinct, which corresponds to the fact that the small time separation can be seen at such high frequencies. Numerical checking of the program included runs using different contours, runs around the poles, runs around closed loops, etc. The fractional error appears to be about 0.1% of the amplitude computed.

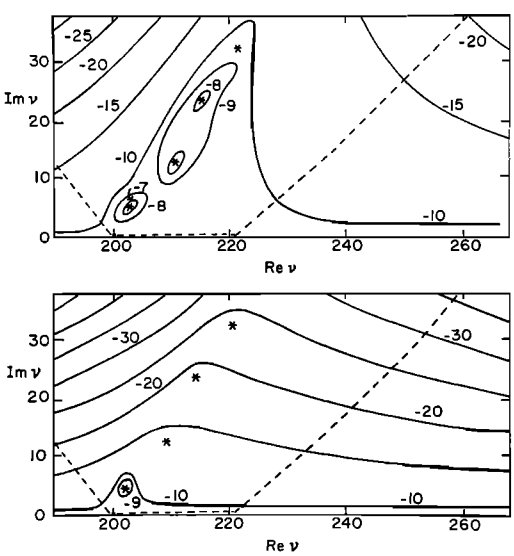

Fig. 1. 'Mixed' core boundary. Maps of the function Re (ln f), where f is the integrand of equation 3. (*Top*) $\theta = 105°$ (illuminated zone); (bottom) for 130° (shadow zone), at $ka = 200$. Dashed line is the integration path, which is steepest descent along the two end segments, and passes between the saddle points when $\theta = 105°$. At 130°, the two saddle points have coalesced in the neighborhood of the first pole, but the original contour is used for integration.

Numerical Results

In all cases, the following parameters were used:

Source and receiver radius r	6350 km
Core radius a	3480 km
Mantle	
P velocity	13.6 km/sec
S velocity	7.5 km/sec
Density	5.5
For 'model 1' the core properties are	
P velocity	8.3 km/sec
S velocity	.001 km/sec
Density	9.5
For 'mixed boundary condition' (M)	
u_r, and $\tau_{r\theta}$ vanish at $r = a$	
For 'hollow boundary condition' (H)	
τ_{rr} and $\tau_{r\theta}$ vanish at $r = a$	

The shadow position for this model is at 113.54°. A normalized frequency of $ka = 100$ corresponds to a true frequency of 0.0622 and a true period of 16.1 sec.

At distances beyond the shadow boundary the first pole was located and the residue evaluated at the pole as a check on the numerical integration. As expected, the two results converge as the receiver moves to larger distances.

In Figure 2 we have plotted the diffraction amplitude (as $\log_e$) against epicentral distance for model 1, our reference earth model. For comparison the amplitude of the direct wave ($1/kR$) is shown. In the illuminated zone away from the shadow, the diffraction pattern appears as the incident wave amplitude with a superposed ripple due to the addition of the PcP signal. The ripple is small enough so that only a very well calibrated array could detect it, because the PcP reflection coefficient is not great. At a certain critical distance from the shadow, the screening effect of the core comes

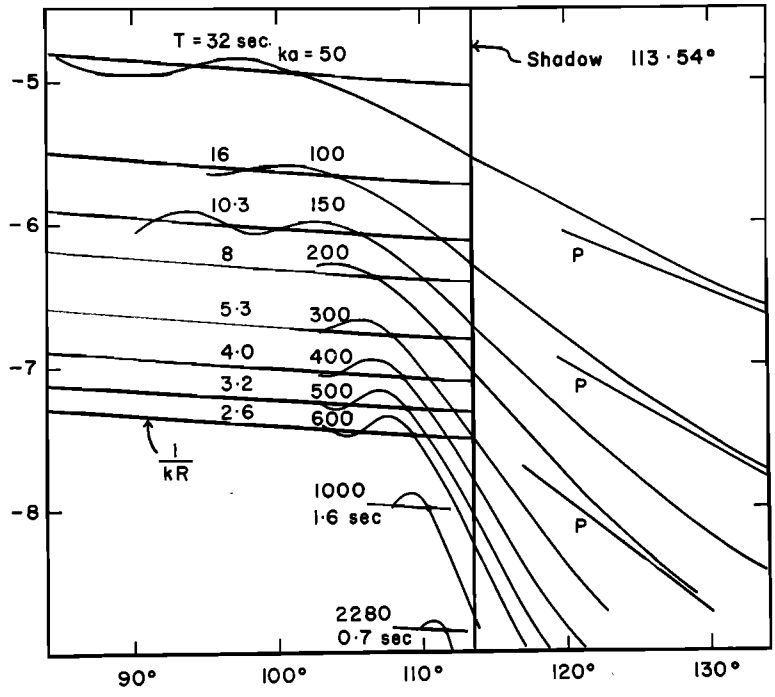

Fig. 2. Natural logarithm of diffraction amplitude for 'model 1.' Straight line (P) in shadow zone give amplitude based on the residue of the first pole. Lines ($1/kR$) in illuminated zone give ray-theoretical amplitude of the incident wave.

into play and the amplitude begins to drop rapidly. The rate of falloff with distance in the transition zone near the shadow is greater than the normal deep-shadow decay given by the lines for the residue solution. This suggests that experimental determination of the deep-shadow decay may be biased by using stations too close to the shadow. The author is not unmindful of the fact that the earlier work with Alexander is subject to this effect, which was allowed for at the time, but was not known numerically.

If the ripple is ignored, these curves resemble the data obtained by *Sacks* [1966], in having a monotonic $1/R$ decrease in the illuminated zone, followed by a sharper monotonic decrease into the shadow. Sacks suggested that the shadow position could be located by identifying the break point at shorter periods, where diffraction effects should be unimportant. We now have a basis for identifying the shadow position at any period by applying a correction to the location of the break point.

Simple physical arguments are available to demonstrate that this break in slope should occur in the illuminated zone, and to provide a scaling law, valid for 'high frequencies.' Consider (Figure 3) a model in which the core is replaced by an opaque screen and assume that the Kirchhoff integration method is adequate to provide the total field at the receiver. It is then appropriate to set up Fresnel zones in the plane of the screen and to inquire at what distance the receiver must lie from the shadow boundary for the first zone to lie off the screen. If we assume that ϕ is small, the path length difference $BAR\text{-}BA'R$, which defines the edge of the first zone, is given by

$$\phi \approx (\tfrac{1}{2}\lambda/BAR_s)^{1/2}$$

This relation gives a square-root scaling law for features in the diffraction pattern near the shadow boundary. When expressed as a discrepancy in the epicentral distance, we have

$$\Delta\theta \cong 2\phi = \left(\frac{2\pi}{ka}\frac{a}{r\sin\tfrac{1}{2}\theta_s}\right)^{1/2}$$

$$\approx 2.0(ka)^{-1/2} = 114.2°(ka)^{-1/2} \qquad (4)$$

In Figure 4, this relationship is plotted along with plots of two characteristic features of the

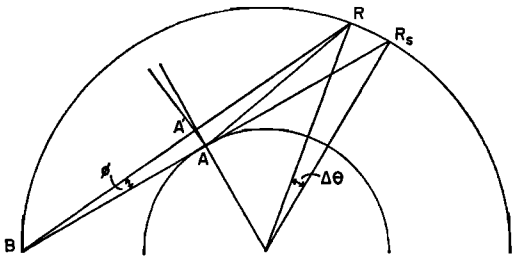

Fig. 3. Geometry for calculation of first Fresnel zone.

diffraction pattern: the distance from breakpoint to shadow and the distance from first peak to shadow. The validity of the square-root law at higher frequencies is verified, although the simplifications in the Fresnel zone model give a modest difference in the actual shift. The square-root scaling law enables a projection to shorter periods and an estimate to be made of the distance between shadow boundary and breakpoint. Extrapolations to periods of 1.6, 1.0, and 0.5 sec give values for the shift of 3.1°, 2.4°, and 1.7°, respectively.

Figures 5 and 6 give the theoretical diffraction amplitude for a 'mixed' and a 'hollow' core, respectively. A comparison of various models is afforded in Figure 7. As mentioned previously [*Phinney and Alexander*, 1966], the mixed boundary condition is the simple model that best approximates the actual situation. Neither looks much like the result for a rigid or hollow core. The close resemblance between the latter two is in agreement with the results of *Knopoff and Gilbert* [1961], who found the rigid and hollow cores indistinguishable from the view of geometrical diffraction theory.

From these results it is possible to infer changes in the shape of the spectrum of a pulse as it transits the shadow edge. At points a few degrees inside the illuminated zone frequencies lower than a certain value are attenuated with respect to the higher frequencies; this is due to the screening of the low frequencies for which the receiver is in the first Fresnel zone. The spectrum is thus relatively enriched in the high frequencies at such points. At the shadow edge all frequencies are lower by about the same amount, thus restoring the original pulse spectrum, and in the nonilluminated region the high frequencies are more rapidly attenuated, giving a spectrum relatively richer at low frequencies. The magnitude of this effect in the illuminated zone is at best about 20%, however.

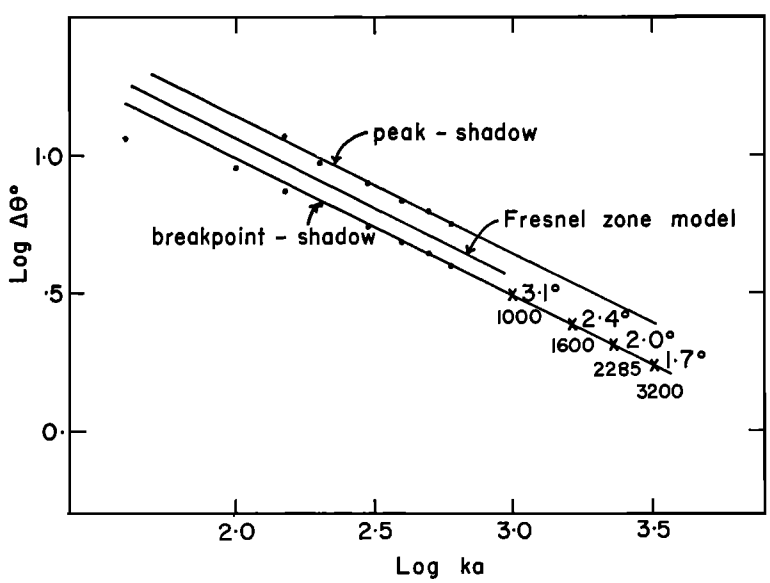

Fig. 4. Scaling of characteristic features of diffraction pattern with frequency. Points are obtained by inspection of Figure 2, and lines are drawn with a slope of $-\frac{1}{2}$. The central line is a plot of equation 4.

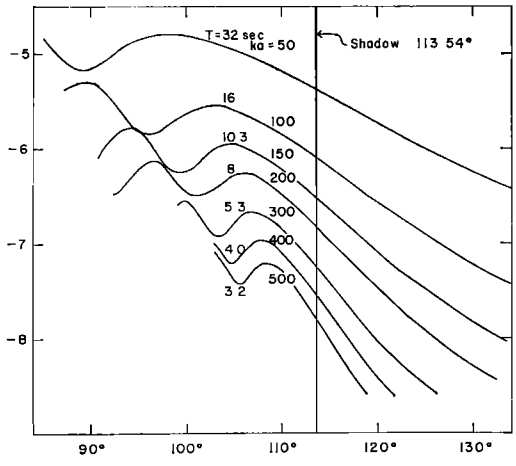

Fig. 5. Natural logarithm of diffraction amplitude for a 'mixed' core.

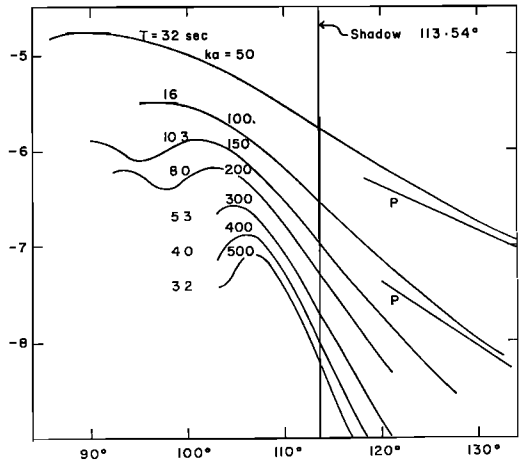

Fig. 6. Natural logarithm of diffraction amplitude for a 'hollow' core.

Comparison with Asymptotic Theory

By taking the frequency sufficiently high, one may form asymptotic expressions for the wave amplitude in various regions. *Nussenzweig*'s [1965] treatment of the acoustic problem may serve as a model for this analysis in the elastic-wave problems of interest. A complete treatment has been performed but is beyond the scope of this paper; we report only the main results. Three regions may be distinguished.

Illuminated zone:

$$\theta = \theta_s - \delta \qquad \delta \gg (ka)^{-1/3}$$

The signal at the receiver is composed of the sum of direct *P* and reflected *PcP*, with phases, amplitudes, and reflection coefficients determined by ray theory.

Transition zone:

$$\theta = \theta_s \pm \delta \qquad \delta \ll (ka)^{-1/3}$$

The signal may be described by the Fresnel

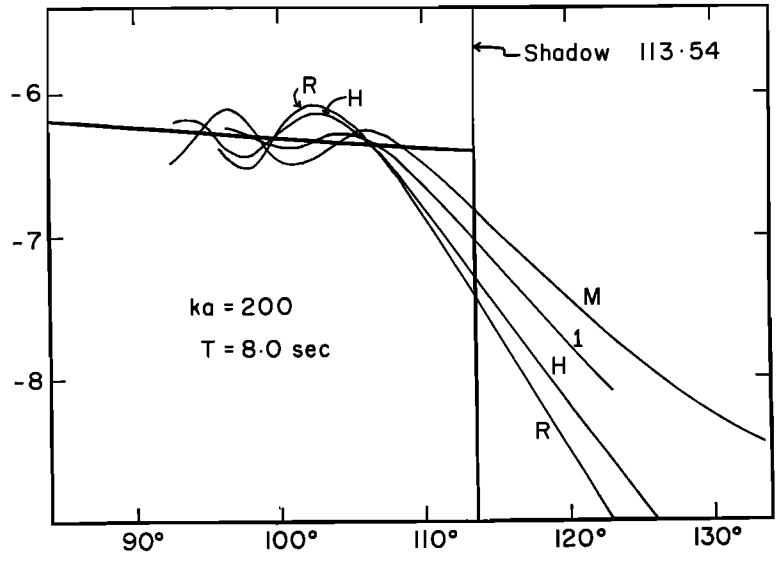

Fig. 7. Comparison of diffraction amplitudes for 'hollow' (H), 'mixed' (M), 'rigid' (R), and 'model 1' (1) cores, at $ka = 200$.

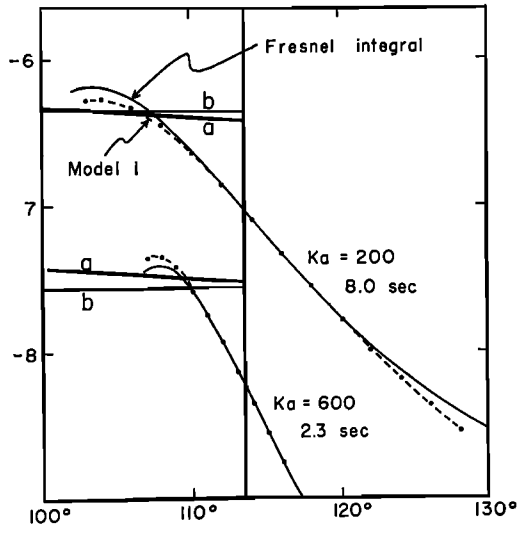

Fig. 8. Comparison of exact (dashed) diffraction amplitudes with those given by the Fresnel integral, for an opaque screen, at $ka = 200, 600$. The lines a and b show the respective ray-theoretical amplitudes.

integral, which gives the classical diffraction pattern of a straight edge, plus a small correction term. *Teng and Richards* [1969] have investigated this theory and expressed their results in terms of an effective shift of the shadow position. They have compared their results with the calculations here reported, and we will not duplicate this discussion.

Shadow zone:

$$\theta = \theta_s + \delta \qquad \delta \gg (ka)^{-1/3}$$

The signal is composed principally of a pole contribution, corresponding to a pulse diffracted along the core-mantle boundary with a given decay constant. The properties of this signal have already been discussed [*Phinney and Alexander*, 1966].

What is of interest in this paper is the determination of a useful form for the amplitude at high frequencies, which gives the transition to shadow. Unfortunately, the above cited theory, whereas valid separately in three regions, is deficient in the gaps between these regions.

We will show here that, despite the theoretical existence of a shadow shift and the theoretical deficiency in patching the regions together, the Fresnel integral so dominates the behavior of the amplitude that it gives a perfectly good representation of our higher-frequency results. This term, as it appears in this problem, has the form

$$\Phi' = \tfrac{1}{2}(e^{-ikR}/ikR)\ D(\Theta) \tag{5}$$

where

$$D(\Theta) = 1 - e^{-i\pi/4}\sqrt{2}\int_0^{\Theta} \exp\left[\frac{i\pi\tau^2}{2}\right] d\tau \tag{6}$$

$$\Theta = (kR/4\pi)^{1/2}(\theta - \theta_s)$$

is the Fresnel integral [*Abramowitz and Stegun*, 1965] which, by itself, gives the amplitude in the neighborhood of an opaque screen. It is seen that (5) provides the square-root scaling inferred on physical grounds in a previous paragraph. In Figure 8 we show the model 1 theo-

TABLE 1. Fresnel Integral Function $D(\Theta)$
For use with equations 5 and 6 to construct an approximate theoretical amplitude across the shadow boundary.

Θ	$D(\Theta)$	ln $D(\Theta)$	Remarks
	2 000	0.697	Asymptotic value
−1 5	2.156	0.768	Illuminated region
−1 4	2 236	0.817	
−1.3	2.325	0.844	
−1.2	2.341	0 850	First maximum
−1 1	2.312	0 838	
−1.0	2 244	0.808	
−0 9	2.147	0 764	
−0 8	2.028	0.707	
−0.7	1.896	0.639	
−0.6	1.756	0.563	
−0.5	1.615	0.479	
−0.4	1.476	0 388	
−0 3	1.344	0.296	
−0.2	1.220	0.199	
−0.1	1.105	0.099	Illuminated region
0.	1.000	0 000	Geometrical shadow position
0.1	0.905	−0.099	Shadow region
0 2	0.820	−0.199	
0.3	0.743	−0.297	
0.4	0.676	−0.392	
0.5	0.616	−0.485	
0.6	0 563	−0.575	
0.7	0 516	−0.662	
0 8	0.474	−0 746	
0.9	0.438	−0.826	
1.0	0.4053	−0.902	Deep shadow entries at reciprocal integers
1 1111	0.3736	−0.985	
1 2500	0 3394	−1.080	
1.4285	0 3026	−1.196	
1 6667	0.2634	−1.333	
2 0000	0 2221	−1.504	
2.5000	0.1790	−1.715	
3 3333	0.1348	−2 004	
5 0000	0 0900	−2 408	
10.0000	0 0450	−3.101	Shadow region

retical curves for $ka = 200$ and $ka = 600$, and compare them with (6). The amplitudes are arbitrarily taken equal at the shadow position; if they were matched by the ray-theoretical values at the shadow, a slight shift of the patterns would be seen. In any case, we find that the Fresnel integral can be used as a short-period representation, for periods less than about 8 sec, with errors that lie in the noise of existing data networks (Table 1).

The other models of the core-mantle boundary do not show as good an agreement (compare Figures 7 and 8). The elastic parameters of the real earth seem fortuitously to give the ideal behavior of an opaque screen. This may be understood by noting that the acoustic impedances $\rho\alpha$ of core and mantle are quite well matched, resulting in relatively little reflection by the boundary. If this reflection is ignored, the field at a receiver may be expressed as a Fresnel-Huygens integral over the portion of the wavefront not screened by the core, leading directly to (5) [*Born and Wolf*, 1965].

Shadow Position

It is clear that shorter periods must be used to make any kind of precise determination of the shadow position. The data discussed later in this paper are all long-period data; therefore, we will rediscuss the results reported by *Sacks* [1966]. He measured amplitudes in the time domain, taking signals that were band-limited by the seismometer. To the extent that the amplitudes of these wave packets are good estimates of Fourier amplitudes, his plot of amplitude decay at three periods is a proper one. The frequency-dependent resonances due to structure found by *Alexander and Phinney* [1966] are certainly minor and offer some reason to believe that Sacks' results are a good representation. Other difficulties with this time domain frequency analysis may arise in the illuminated zone, owing to the lagged superposition of *P* and *PcP*, but here the small *PcP* reflection coefficient minimizes the problem.

In Figure 9, Sacks' results are plotted for comparison with our computed diffraction patterns. Two degrees of freedom are available: the amplitude and the angle scale. Since we have made no independent determination of the frequency content of the signal, the scale factor for each frequency is arbitrary and may be chosen to get a good fit. The two angle scales are not the same, since the theoretical model does not take account of the variable velocity in the mantle and has a different position for the shadow. Knowing that the distortion of

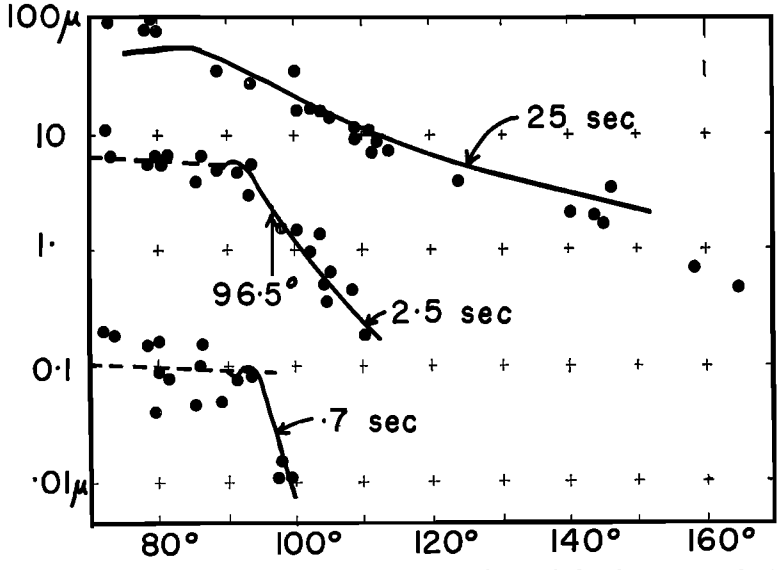

Fig. 9. Diffraction amplitude estimated by Sacks for periods of 25, 2.5, and 0.7 sec. The curves are our theoretical amplitudes for these periods (model 1) with amplitude and distance adjustments as described in the text.

wavefronts by the velocity distribution in the lower mantle is not 'too severe,' we find that the error involved in simply translating the theoretical curve a few degrees to match the position of the shadow with that of the real earth is acceptably small. (Future data analyses may require that the mantle structure be included in the theory in a reasonable way.) A full discussion of this point may be based on a WKBJ treatment of the wave function in the mantle.

The placement of the theoretical curves on Figure 9 is done in the following way:

1. The amplitude of the theoretical curve for 2.5 sec is scaled to agree with the data at 80°, which is in the illuminated zone. The ripple being small, the theoretical curve here is just $1/kR$, which fortuitously decays in about the same way as real ray amplitudes in this region. The abscissa is now shifted to afford the best agreement with the data in the shadow. The fit in shape is as good as the data scatter will permit. The abscissa shift brings the shadow position to 96.5°.

2. The theoretical curve for 25 sec is directly plotted, using the scale adjustments determined for the 2.5-sec data. Beyond 86° the fit is quite good. Since an independent amplitude adjustment was not necessary, we have coincidentally found that the spectrum of the earthquake had the $1/k$ (step) behavior assumed in the theoretical model, with respect to these two periods.

3. Using the Fresnel integral, we can con-

TABLE 2. Source Parameters and Station Distances and Azimuths for Brazil Earthquake

Time, 21h 15m 30.4s November 9, 1963; location, west Brazil, 9.0°S, 71.5°W; magnitude, 6.8; depth, 600 km.

Station	Distance	Azimuth
PTO	76.4°	43.9°
TOL	79.0°	46.4°
STU	90.6°	40.7°
AQU	92.3°	47.6°
KON	93.2°	47.6°
NOR	93.9°	7.1°
NUR	100.8°	30.1°
KEV	101.3°	20.5°
IST	103.8°	50.0°
HLW	105.5°	61.5°
NAI	107.5°	94.6°
SHI	123.7°	60.7°
QUE	135.8°	55.8°
NDI	144.7°	52.6°
SHL	157.1°	42.8°

TABLE 3. Source Parameters and Station Distances and Azimuths for Taiwan Earthquake

Time, 8h 50m 2.2s, February 13, 1963; location, Taiwan, 24.5°N, 121.8°E; magnitude, 7.2; depth, shallow.

Station	Distance	Azimuth
	LRSM Stations Used in Taiwan-North America Analysis	
WINV	94.5	40.5
TFCL	96.7	46.6
KNUT	100.1	41.5
CPCL	100.6	46.8
FSAZ	102.3	42.2
WNSD	102.3	30.0
DRCO	102.7	38.4
SEMN	103.7	26.0
HBOK	109.2	34.5
SSTX	111.2	40.4
GVTX	112.0	34.7
MPAR	112.5	30.8
BLWV	114.3	20.0
MMTN	114.9	24.4
	WWSSN Stations Used in Taiwan-North America Analysis	
CCG	78.5	1.0
BKS	93.7	45.4
GOL	102.4	35.4
MNN	103.9	24.8
TUC	104.4	44.0
MDS	106.4	23.5
LUB	108.8	37.5
AAM	109.5	19.7
FLO	110.2	26.3
DAL	112.1	34.5
WES	112.3	10.5
GEO	114.5	16.1
BLA	115.1	19.5
SHA	118.1	29.1
BEC	123.1	6.6
CAR	144.2	14.7
TRN	144.9	5.5
QUI	148.9	41.7
	Stations Used in Taiwan-Europe Analysis	
COP	80.3	327.2
ATU	81.3	307.7
STU	85.5	322.2
AQU	86.3	315.2
VAL	93.1	333.0
MAL	100.8	318.7
BUL	100.8	253.0
PRE	103.3	248.0

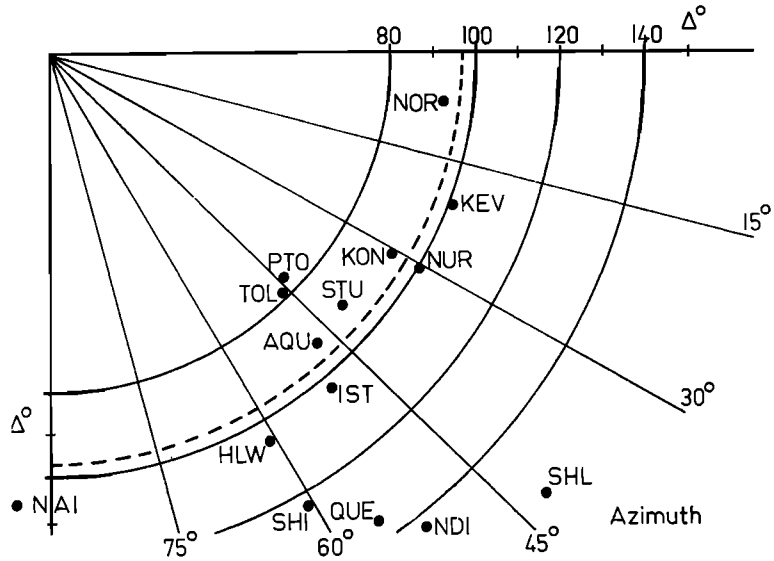

Fig. 10. Brazil earthquake of November 9, 1963: Plot of stations used in the amplitude study.

struct a theoretical pattern for 0.7 sec. If plotted using the scale adjustments of the 2.5-sec data, the amplitude would be too large by a factor of 12. Making an independent amplitude shift, then, we plot the theoretical 0.7-sec curve to match the data in the illuminated zone. The dropoff of amplitude into the shadow is seen to take place at the right distance.

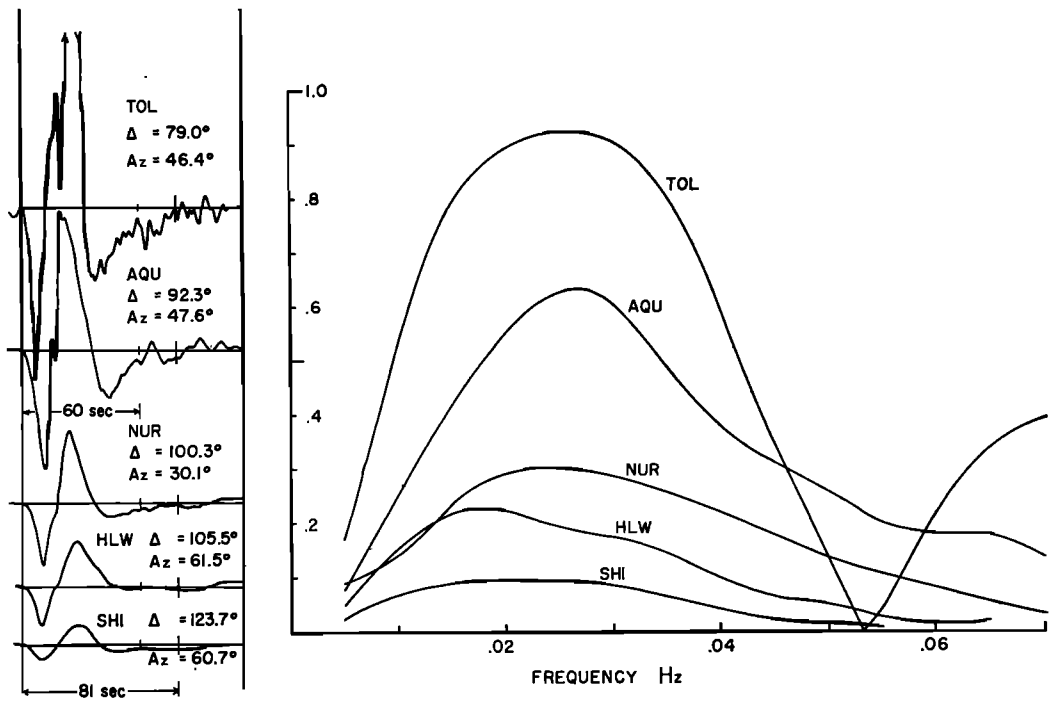

Fig. 11. Brazil earthquake of November 9, 1963: Representative time signals and their amplitude spectra.

Whereas the 25- and 0.7-sec results are interesting, the 2.5-sec result is more constrained, owing to the availability of data on both sides of the break in slope and to the sharpness of the break. To the extent that a single interface is a good model of the core-mantle boundary, we find a shadow position of 96.5°, essentially in agreement with Sacks.

It is worth noting that precise knowledge of the shadow position is not equivalent to a better determination of core radius. Either the velocity profile at the base of the mantle or the radius of the core may be independently adjusted to bring about a desired shadow position. The very different effect of the velocity profile on near-vertical *PcP* and on near-grazing *P* indicates the desirability of a study that jointly rationalizes both types of data. A number of authors have contributed to the solution of this problem in the past few years. In this paper no position is taken regarding the core radius.

Analysis of Data

To provide some notion of the behavior of real amplitudes for comparison with the theory, data from two earthquakes, involving three different paths, have been analyzed to determine the behavior of their Fourier components near the shadow boundary. Tables 2 and 3 and Figures 10, 14, and 18 characterize the sources and array characteristics. As far as permitted by the distribution of stations, each analysis was chosen to involve a restricted range of azimuths and thus to eliminate effects of the radiation pattern.

Preliminary processing involved digitizing (about 1/sec) and removal of trend for a time window somewhat in excess of the pulse length. For these two events the reverberation following the pulse is low enough so that selection of a cutoff offers no problems, and the spectrum can be regarded as a Fourier integral spectrum, defined for continuous frequency, but smooth according to the pulse length. The presentation of the results for frequencies of 0.02, 0.03, ⋯, 0.07 reflects the band containing significant energy and the limited number of independent spectral values possible for the time window used. Amplitude calibration was employed for the Long Range Seismic Measurements (LRSM) network data, using information supplied with the data. Data from the World-Wide Standard Seismological Network (WWSSN) were taken from 15× reproductions of the 70-mm film chips; the nominal magnification was used for calibration unless the calibration pulse fell outside 10% limits. Stations with anomalous calibration time constants were not used. This approach follows our observation that most of the scatter in the final results was not attributable to instrument calibration (or radiation pattern, for that matter). Other stations were deleted because of high noise levels, unstable base lines, or grossly unexplainable discrepancies.

The data were then Fourier-transformed.

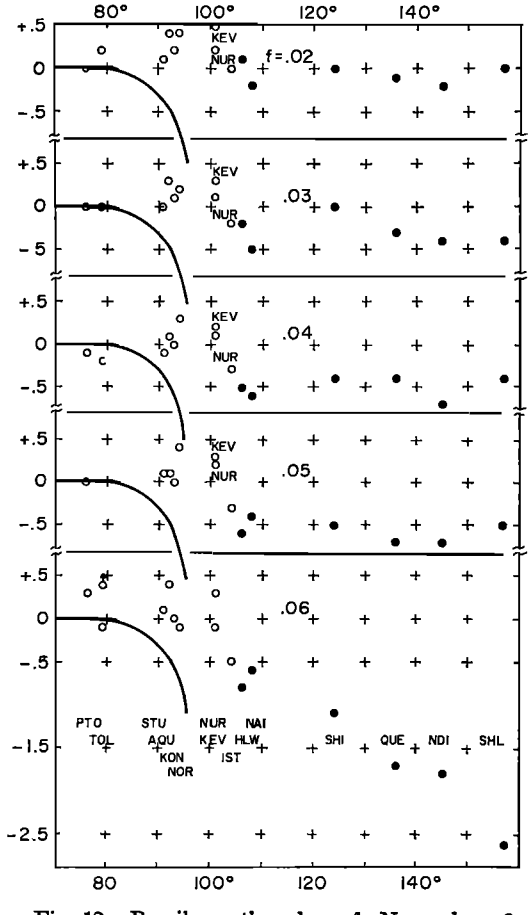

Fig. 12. Brazil earthquake of November 9, 1963: Spectral amplitude residuals with respect to the model 1 theoretical diffraction amplitude, for a shadow at 96.5°. Ordinate units are in natural logarithms, or about 8 db per unit. Solid dots represent points used in determining the deep shadow decay (Figure 13).

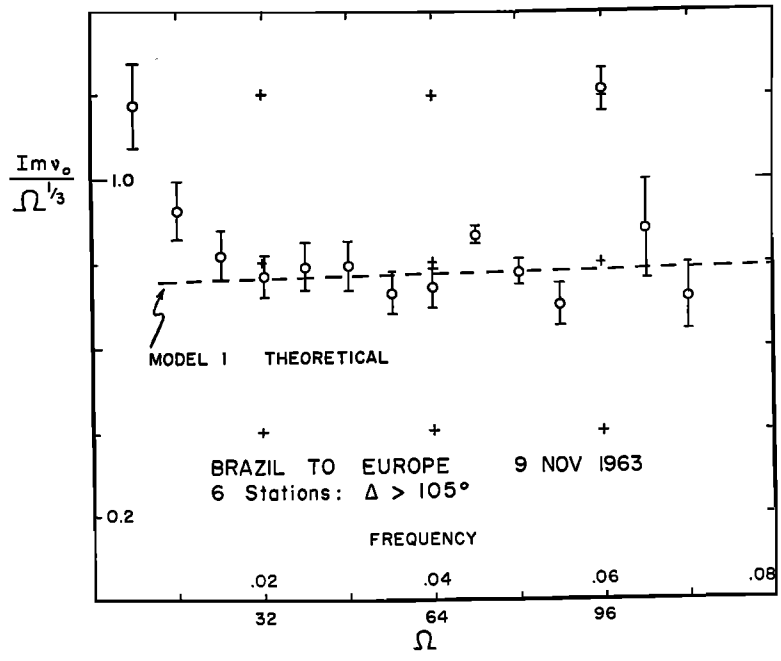

Fig. 13. Brazil earthquake of November 9, 1963: Spatial decay in deep shadow normalized by $(ka)^{1/3}$. Error brackets give the formal standard deviation of a least-squares fit to the data. Dashed curve gives the theoretical behavior of a model 1 earth.

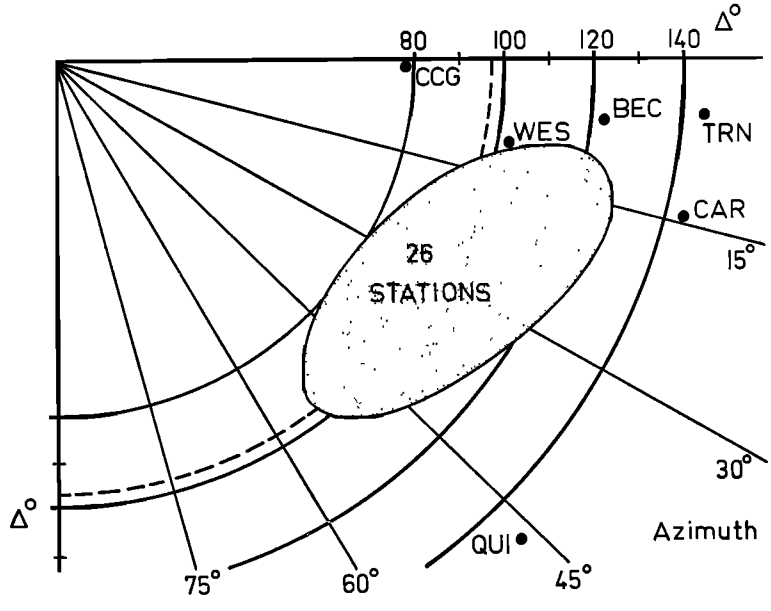

Fig. 14. Taiwan earthquake of February 13, 1963: Plot of stations used in the amplitude study, for azimuths to North America.

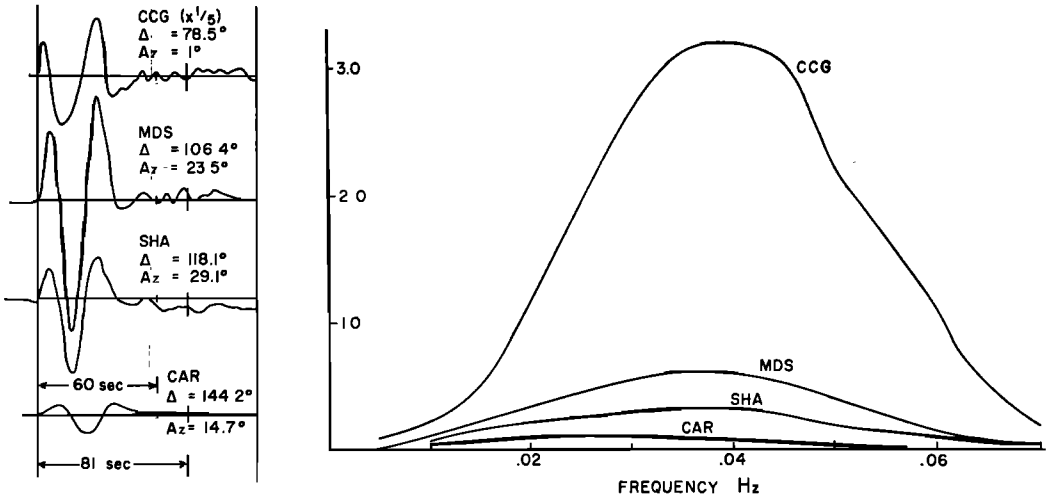

Fig. 15. Taiwan earthquake of February 13, 1963: Representative time signals and amplitude spectra; for azimuths to North America. Ordinates are plotted to a scale consistent with that used in Figure 11, except for CCG (× 1/5).

Figures 11, 15, and 19 show representative time signals and their amplitude spectra. It is then appropriate to form a plot of amplitude for each frequency as a function of distance. Diffraction amplitudes must look very much like those shown in Figure 2, with possible perturbations superposed, owing to departures from the model 1 earth. Consequently, they are plotted as residuals against the nominal model 1 diffraction amplitudes. This processing requires:

1. The theoretical amplitudes are transformed to natural logarithms, and ½ ln (sin θ) subtracted, to eliminate focusing due to the spherical geometry. This scale is taken so that the ray-theoretical amplitude $1/kR$ is at zero for $\theta = 90°$ (model 1 earth). These functions, tabulated in Table 4, may be used as a standard for comparison of data.

2. The experimental amplitudes are transformed to natural logarithms and similarly corrected for focusing. The scale is set to zero at a selected station in the illuminated zone.

3. The residual, experimental-theoretical, is formed and plotted in Figures 12, 16, and 20. For this purpose, the theoretical pattern is shifted to give a shadow position of $\Delta = 96.5°$, in agreement with our discussion of the 2.5-sec results.

A special problem exists in plotting the results from two networks together because of the differing instrument responses. In this case, for Taiwan to North America (Figure 16), one assumes that the signal is identical at two proximate stations from the two networks, and corrects all LRSM spectral amplitudes to the WWSSN response on the basis of the observed spectra at the two stations. GOL and DRCO were used for this adjustment; other proximate station pairs, such as LUB-HBOK and BLA-BLWV then plot with good agreement, providing some validation of the procedure.

Discussion

These results are plotted to permit small effects in the ordinates, including scatter, to be amplified. The main effect is agreement with the theoretical diffraction, manifest as points lying on a horizontal. Further systematic effects due to structure of some sort in the core-mantle region should be apparent, if present and if proper allowance could be made for the crust-upper mantle correction at each station.

As mentioned, we find that refined calibration does not reduce the scatter, which amounts to 0.2–0.4, or about 3 db. The present advisability of a correction for crustal response [*Haskell*, 1962] may be questioned. It may be shown [*Alexander and Phinney*, 1966] that to first order all stations have the same crustal correction to 10%, in this long-period band, due to their situation on crust of approximately the

same thickness. Although admittedly unsatisfactory, we find this preferable to applying *P*-wave spectral corrections that are based on an extremely heterogeneous body of information about crustal structure. The only consistent way to make this correction is to use the *P* waves themsleves as calibrators, using a variety of earthquakes and studying ratios between station pairs and between individual components. It is quite likely that a major cause of amplitude variation is scintillation caused by velocity heterogeneity in the upper mantle. Short-period amplitude and travel time calibration of the LASA array in Montana [*Broome*, 1967] encourages this view and demonstrates the strong dependence of the corrections on azimuth and angle of incidence.

Certain anomalies in the amplitude residuals might be discerned, although we do not insist too strenuously on their reality. The best of these is a pronounced increase in the decay rate in the shadow, seen at 0.06 Hz in the Brazil-Europe analysis (Figure 12). Figures 13 and 17 show an analysis of this decay for the two regions having suitably located stations. Aside from the 0.06 point, which may be real and which might be explained with the requisite ingenuity, the remainder of the Brazil decay spectrum is quite nominal, a confirmation of the result for this path obtained by *Alexander and Phinney* [1966]. The Taiwan-North America decay spectrum (Figure 17) is anomalously high, again in agreement with the earlier results from the North Pacific, although the reader can judge the degree to which this result is dependent on the choice of stations for analysis. For both paths, one might discern a drop of 0.3 and 0.5 in the amplitude residual at 105° and 115°, respectively (Figures 12 and 16). Such an effect, if real, cannot be due to perturbations in the shadow position produced by variations in lower mantle structure; this possibility is ruled out by the drop's being sharp at these long periods. One can postulate a lateral reflector or scatterer at the base of the mantle or a major region of defocusing due to shallower mantle inhomogeneity.

Teng [1968] studied the *Q* structure of the lower mantle by comparing spectra within a group of stations. The question of whether his data require a low-*Q* zone at the base of the mantle hinges on the extent to which diffraction effects were fully accounted for. Data scatter is a problem here, too. A full correction would require taking residuals with respect to our nominal diffraction amplitudes before computing the *Q*-related effects.

We have shown that diffraction effects penetrate several degrees (depending on frequency) into the illuminated zone, giving an amplitude drop of a factor of 2 in this region. Amplitude decrease beyond about 85° has long been noticed in conventional *P*-wave amplitude studies that use time domain measurements and ray theory interpretations. It is not possible to convert such published amplitudes into a form comparable with the frequency-dependent theory. Some discussion is still possible. We note that

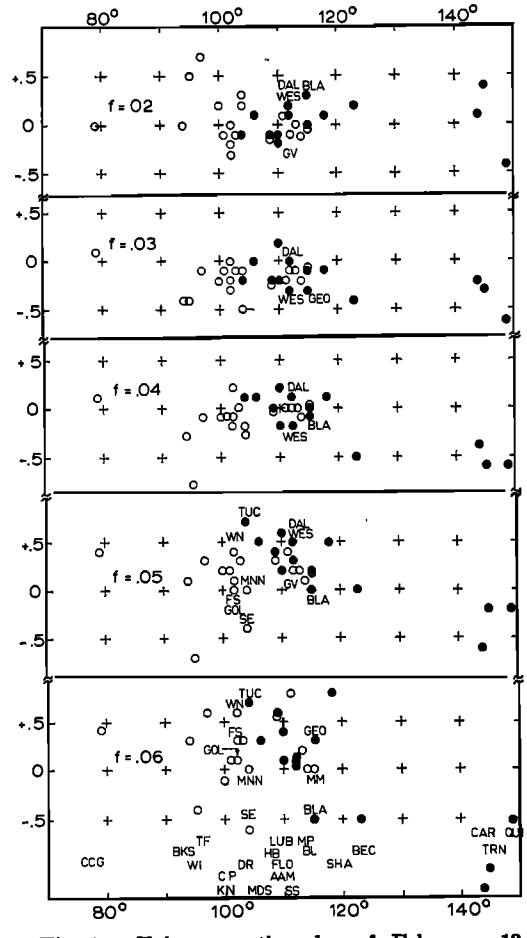

Fig. 16. Taiwan earthquake of February 13, 1963: Spectral amplitude residuals for azimuths to North America, plotted with the same conventions as in Figure 12.

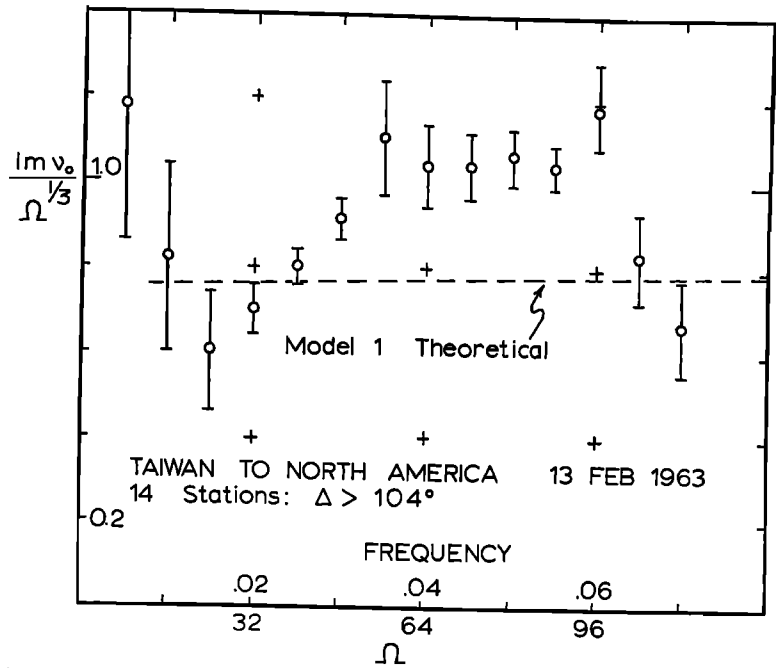

Fig. 17. Taiwan earthquake of February 13, 1963: Spatial decay for azimuths to North America, plotted with the same conventions as in Figure 13.

the square-root scaling of the diffraction pattern at intermediate and high frequencies implies relatively little shift in the pattern the higher the frequency. Even at 1 Hz, normally used in amplitude studies, the amplitude is expected to begin dropping 2.5° short of the shadow position. Figure 21 compares a recent amplitude curve by *Cleary* [1967] with diffraction theory for 0.03 and 0.25 Hz. If the signals used were in this frequency range, diffraction may fully account for the observations. Cleary also found essential agreement between his observed amplitudes and the values predicted from the structure of the observed travel times

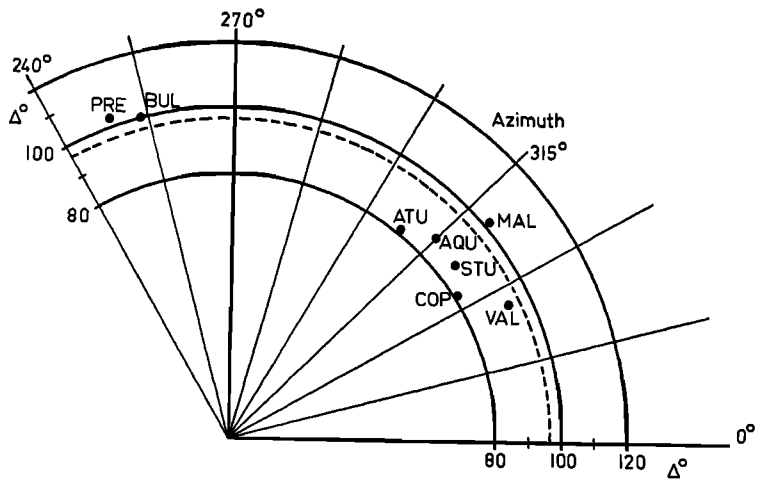

Fig. 18. Taiwan earthquake of February 13, 1963: Plot of stations used in the amplitude study, for azimuths to Europe.

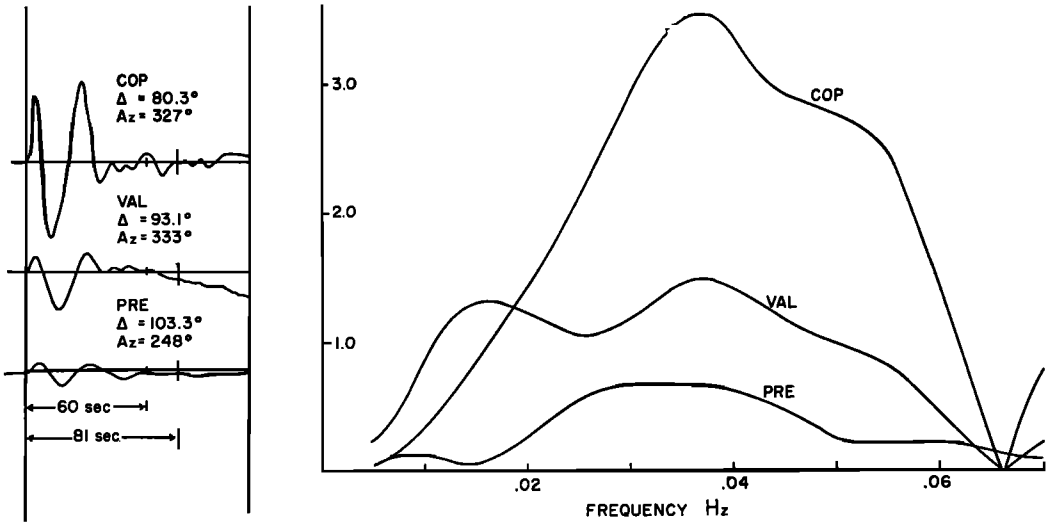

Fig. 19. Taiwan earthquake of February 13, 1963: Representative time signals and amplitude spectra, for azimuths to Europe. Spectral ordinates are consistent with Figures 11 and 15; time signal ordinates are consistent with a scaling of 1/10.

TABLE 4. Theoretical Diffraction Amplitude for Model 1, for Use in Forming Data Residuals

The arbitrary zero of ordinates is set so that the ray-theoretical amplitude $1/kR$ is at zero at 90° in the model earth. For this tabulation the epicentral distances are given for the model 1 parameters and shifted to correspond to a shadow position of 96.5°, for the real earth. The $(\sin \Theta)^{\frac{1}{2}}$ has been taken out.

Model 1 Distance $\Theta_s = 113.5°$	Shifted Distance for Real Earth $\Delta_s = 96.5°$	Natural Log of Diffraction Amplitude						
		$ka = 32$ $f = .02$	$ka = 48$ $f = .03$	$ka = 64$ $f = .04$	$ka = 80$ $f = .05$	$ka = 96$ $f = .06$	$ka = 112$ $f = .07$	$ka = 128$ $f = .08$
90°	73°	0.023	−0.092	−0.094	0.018	0.104	0.092	−0.011
92°	75°	0.037	−0.049	−0.116	−0.090	−0.003	0.067	+0.078
94°	77°	0.032	−0.013	−0.080	−0.122	−0.106	−0.047	0.014
96°	79°	0.010	+0.000	−0.038	−0.085	−0.119	−0.124	−0.099
98°	81°	−0.030	−0.013	−0.021	−0.044	−0.074	−0.103	−0.124
100°	83°	−0.083	−0.051	−0.037	−0.035	−0.042	−0.057	−0.076
102°	85°	−0.149	−0.111	−0.085	−0.066	−0.054	−0.049	−0.049
104°	87°	−0.224	−0.189	−0.159	−0.134	−0.112	−0.094	−0.080
106°	89°	−0.308	−0.281	−0.256	−0.231	−0.208	−0.187	−0.169
108°	91°	−0.397	−0.384	−0.368	−0.352	−0.334	−0.318	−0.302
110°	93°	−0.492	−0.495	−0.493	−0.489	−0.482	−0.474	−0.466
112°	95°	−0.590	−0.612	−0.626	−0.636	−0.643	−0.648	−0.650
114°	97°	−0.691	−0.732	−0.764	−0.790	−0.811	−0.829	−0.843
116°	99°	−0.793	−0.855	−0.905	−0.947	−0.981	−1.012	−1.038
118°	101°	−0.895	−0.977	−1.045	−1.102	−1.150	−1.192	−1.230
120°	103°	−0.998	−1.100	−1.184	−1.255	−1.315	−1.369	−1.419
122°	105°	−1.099	−1.220	−1.320	−1.403	−1.474	−1.540	−1.599
124°	107°	−1.200	−1.339	−1.453	−1.547	−1.629	−1.705	−1.772
126°	109°	−1.300	−1.456	−1.582	−1.687	−1.780	−1.864	−1.936
128°	111°	−1.398	−1.570	−1.707	−1.823	−1.925	−2.016	−2.095
130°	113°	−1.495	−1.682	−1.829	−1.955	−2.066	−2.163	−2.251
132°	115°	−1.590	−1.791	−1.948	−2.084	−2.203	−2.305	−2.402
134°	117°	−1.684	−1.898	−2.065	−2.211	−2.335	−2.447	−2.550
136°	119°	−1.777	−2.003	−2.180	−2.335	−2.466	−2.586	−2.694
138°	121°	−1.869	−2.106	−2.294	−2.457	−2.595	−2.723	−2.835
140°	123°	−1.959	−2.208	−2.406	−2.576	−2.724	−2.857	−2.977
142°	125°	−2.049	−2.309	−2.517	−2.695	−2.852	−2.988	−3.118
144°	127°	−2.137	−2.409	−2.628	−2.812	−2.978	−3.119	−3.258
146°	129°	−2.225	−2.508	−2.737	−2.930	−3.103	−3.251	−3.396
148°	131°	−2.312	−2.607	−2.845	−3.048	−3.226	−3.385	−3.532

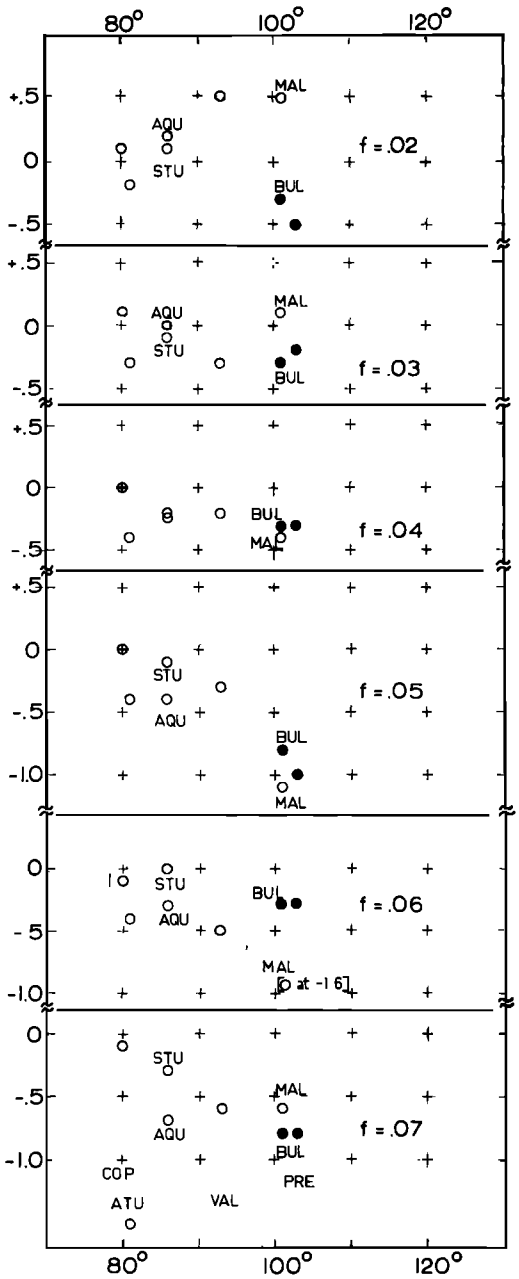

Fig. 20. Taiwan earthquake of February 13, 1963: Spectral amplitude residuals for azimuths to Europe, plotted with the same conventions as in Figure 12.

(through $d^2T/d\theta^2$), on a ray-theoretical interpretation.

Amplitude distortion implies phase distortion in a linear realizable system; we may thus determine the departures of the P-wave phase velocity from ray theory directly from the originally computed phase spectrum. Figure 22 represents this as a function of frequency and distance. It is now possible to compute the amplitude expected from these phase velocities under the (false) assumption of ray optics. That computed amplitude is seen (Figure 21) to be quite similar to the correct diffraction amplitude. Thus, despite the cross-checking of the amplitude data with the travel-time data, Cleary may not have been seeing ray-optical defocusing at all.

It is of some interest to look for the phase-velocity distortion in our long-period data. Using the Kermadec earthquake of May 20, 1963, four stations were Fourier-analyzed. The phase spectrum was converted to a phase 'arrival time' at each frequency, and this was added to the starting time of the window. In plotting, a straight line with a slope of 24.82 km/sec was subtracted from the data and residuals were plotted (Figure 23). At the greater distances, the lower frequencies are seen to have slightly lower phase velocities. In general, however, this is a fairly delicate measurement, made more so by the expected variation of phase velocity with distance. *Sacks* [1967] has attempted most recently to fix the phase velocity by time domain measurements on diffracted waves; his determination of 24.55 ± .08 km/sec lies within the scatter of our results. Both studies have used long periods, however. Figure 22 suggests that the true high-frequency value might be underestimated by 1 km/sec.

In conclusion, it should be noted that we are reluctant in this paper to engage in modeling of the actual core. This has been the object of much recent attention. Our objective here is to make available a more correct physical description of the shadowing process and to indicate by examples the types of data analysis affected. In general, we have reservations about the use of time domain measurements on data that are easily described only in the frequency domain, especially when the measurement being attempted is quite delicate. In fact, it is not clear that even present networks have the usable bandwidth and calibration quality needed to do high-resolution studies of the core, even in the frequency domain.

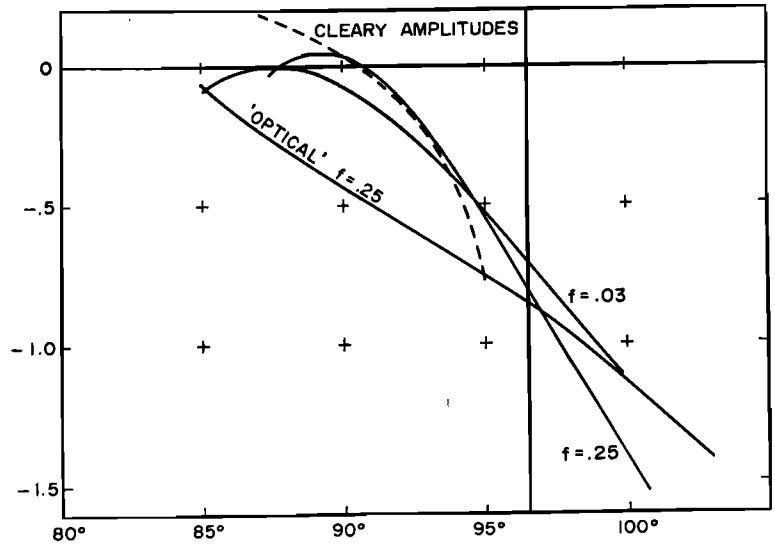

Fig. 21. Comparison of Cleary and Hales amplitudes with diffraction theory. 'Optical' curve is computed from the phase distortion of diffraction theory under ray-optic assumptions.

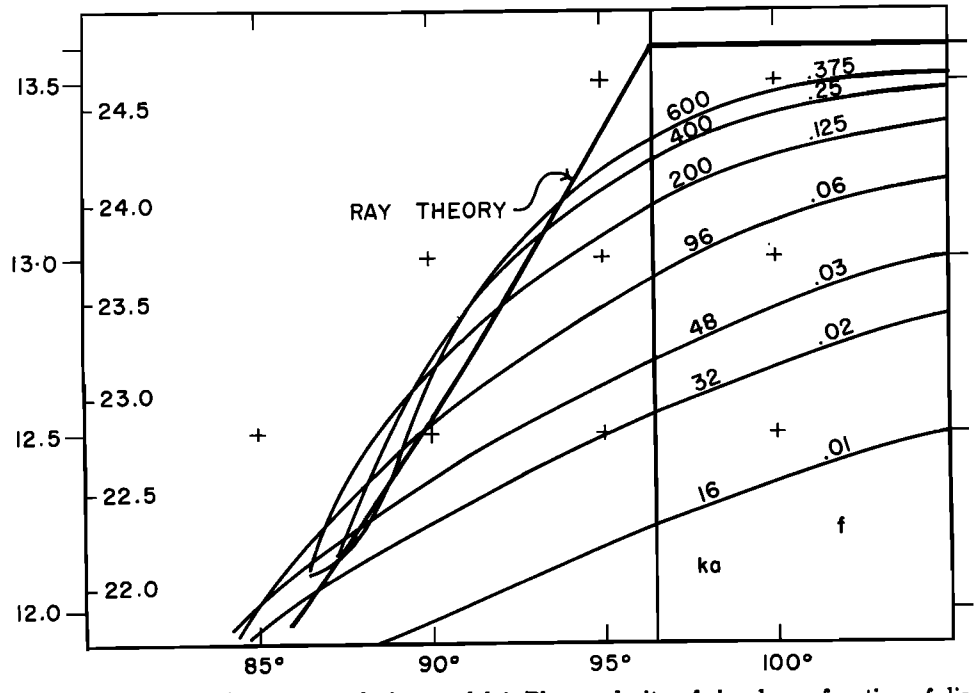

Fig. 22. Analysis of apparent velocity, model 1. Phase velocity of signal as a function of distance and frequency. Left-hand ordinate is phase velocity reduced to base of mantle.

Acknowledgments. This work was supported by the Air Force Office of Scientific Research under contract AF 49(638)-1243. The computer facilities were partly supported by National Science Foundation grant GP 579. Digitized data from the Long Range Seismic Measurements network were supplied by the Teledyne Seismic Data Laboratory, Alexandria, Virginia.

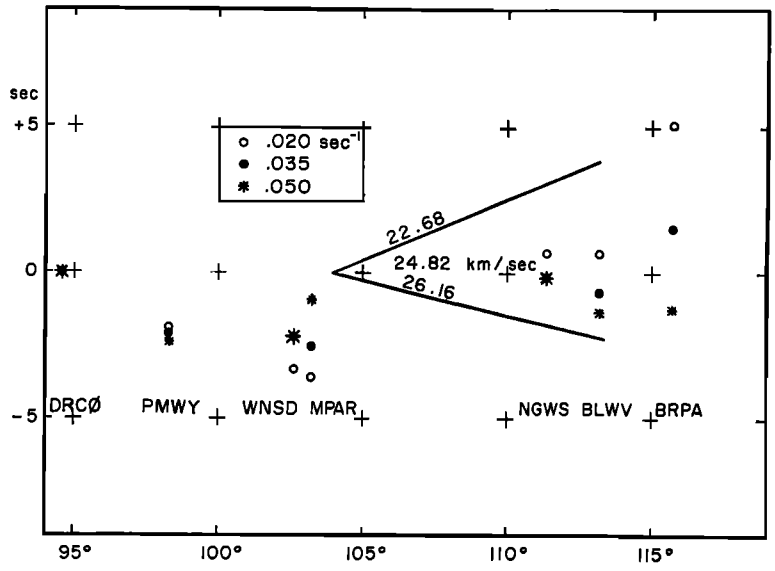

Fig. 23. Kermadec earthquake of May 20, 1963: Comparison of residual phase arrival times for three frequencies.

References

Abramowitz, M., and I. A. Stegun, Ed., *Handbook of Mathematical Functions,* 1046 pp., Dover, New York, 1965.

Alexander, S. S., and R. A. Phinney, A study of the core-mantle boundary using *P* waves diffracted by the earth's core, *J. Geophys. Res., 71*(24), 5959–5975, 1966.

Born, M., and E. Wolf, *Principles of Optics,* 3rd ed., 808 pp., Pergamon Press, New York, 1965.

Bremmer, H., *Terrestrial Radio Waves,* Elsevier, Amsterdam, 1949.

Broome, P. W., Amplitude anomalies at LASA, *Teledyne Co. Rept. LL-7,* Alexandria, Virginia, August 9, 1967.

Cleary, J., Analysis of the amplitudes of short-period *P* waves recorded by long range seismic measurements stations in the distance range 30° to 102°, *J. Geophys. Res., 72*(18), 4705–4712, 1967.

Duwalo, G., and J. A. Jacobs, Effects of a liquid core on the propagation of seismic waves, *Can. J. Phys., 37,* 109–128, 1956.

Haskell, Norman A., Crustal reflection of plane *P* and *SV* waves, *J. Geophys. Res., 67,* 4751–4767, 1962.

Knopoff, L., and F. Gilbert, Diffraction of elastic waves by the core of the earth, *Bull. Seismol. Soc. Am., 51*(1), 35–50, 1961.

Morse, P. M., and M. Feshbach, *Methods of Theoretical Physics,* McGraw-Hill, New York, 1953.

Nussenzweig, H. M., High-frequency scattering by an impenetrable sphere, *Ann. Phys., 34,* 23–95, 1965.

Phinney, R. A., and S. S. Alexander, *P* wave diffraction theory and the structure of the core-mantle boundary, *J. Geophys. Res., 71*(24), 5943–5958, 1966.

Sacks, I. S., Diffracted wave studies of the earth's core, 1, Amplitudes, core size, and rigidity, *J. Geophys. Res., 71,* 1173–1182, 1966.

Sacks, I. S., Diffracted *P*-wave studies of the earth's core, 2, Lower mantle velocity, core size, lower mantle structure, *J. Geophys. Res., 72*(10), 2589–2594, 1966.

Scholte, J. G. J., On seismic waves in a spherical earth, *Koninkl. Ned. Meteorol. Inst. Publ., 65,* 1956.

Teng, T. L., Attenuation of body waves and the *Q* structure of the mantle, *J. Geophys. Res., 73*(6), 2195–2208, 1968.

Teng, T. L., and P. G. Richards, Diffracted *P, SV,* and *SH* waves and their shadow-boundary shifts, *J. Geophys. Res., 74,* this issue, 1969.

Teng, T. L., and F. T. Wu, A two-dimensional ultrasonic model study of compressional and sphere wave diffraction patterns produced by a circular cavity, *Bull. Seismol. Soc. Am., 58*(1), 171–178, 1968.

Watson, G. N., The diffraction of electric waves by the earth, *Proc. Roy. Soc. London, A, 95,* 83, 1918.

(Received August 26, 1968;
revised December 9, 1968.)